Solid-State Electronics 213 (2024) 108849

Contents lists available at ScienceDirect

Solid State Electronics

journal homepage: www.elsevier.com/locate/sse

A unified core model of double-gate and surrounding-gate MOSFETs for circuit simulation

Luigi Colalongo [a,*], Simone Comensoli [b], Anna Richelli [a]

[a] D.I.I., University of Brescia, 25123 Brescia, Italy
[b] PDF Solutions, Desenzano Del Garda, 25015 Brescia Italy

ARTICLE INFO

The review of this paper was arranged by Prof. Alex Zaslavsky
Handling Editor: A. Zaslavsky

Keywords:
Double-gate
Surrounding-gate
MOSFET
SPICE
Surface potential
TCAD

ABSTRACT

This paper presents a new core compact model of double-gate (DGFET) and surrounding-gate (SGFET) MOSFETs for circuit simulations. The current and the terminal charges are continuous with high computation efficiency and accuracy. Despite its accuracy, it retains the same simplicity of the industry standard transistors models. The drain current is worked out without invoking the charge-sheet approximation exploiting a quadratic symmetric polynomial interpolation of the charge in the channel. Apart this clear approximation, no other simplification is used to work out the drain current, the terminal charges, the potential, and electric field in the channel. The accuracy of the model is shown by comparison with the exact numerical solution and experimental data of the literature.

1. Introduction

Double gate, surrounding-gate and, more generally, multiple gate MOSFETs (MGFET) as FINFET and Nano Sheets, are widely used in the electronic industry to replace conventional planar transistors [1] thanks to the improved gate control, near ideal subthreshold slope, and reduced short channel effects (SCE). In principle, these devices have the potential of maintaining the scalability of MOSFETs as the technology approaches the end of the roadmap. Hence, there is a significant interest in developing compact CAD models for circuit simulation [2–15]. A compact CAD model for circuit simulations consists of a core model of an ideal long-channel transistor in which SCE and quantum effects are introduced later as suitable approximations. In the literature, several excellent closed-form equations of the drain current symmetric DGFET and SGFET were worked out [2–15], nevertheless, exact closed-form expressions of the terminal charges are somewhat more complex with respect to planar transistors compact models and requires simplifications. Furthermore, the complexity of the existing MGFET core models is not conducive to the inclusion of SCE. The aim of this work is to present a new core model for DGFET and SGFET based on the exact solution of the Poisson's equation without the charge-sheet approximation. Then, a quadratic symmetric polynomial interpolation is used to work out the transistor current. We show that this approach is particularly suited to accurately model DGFET and SGFET and easily manage terminal charges, capacitances, and small channel effects. It retains all the appealing features of customary compact models of planar MOSFETs as PSP: computational efficiency, symmetry, simple polynomial expression of current, terminal charges, potentials, and electric field in the channel. The advantage of this approach is threefold. First, it is a compact model for circuit simulations and retains the same simplicity of the industry standard transistors models. Second, although compact and easily implementable in circuit simulators, it is very accurate: the largest error compared to the exact solution is so small that the model can be considered equivalent to the exact solution. Third, the terminal charges, capacitances, potential and electric field in the channel are computed exactly: no simplification is required. The model is fully scalable and is suitable full range of device geometries, from the long-channel limit down to the shortest channels, with a single set of parameters. Nevertheless, as stated above, it is only the kernel of the MGFETs compact model; SCE, quantum effects, low and high field transport, noise, etc. should be included when it is used in a circuit simulator (Table 1).

* Corresponding author.
E-mail address: luigi.colalongo@unibs.it (L. Colalongo).

https://doi.org/10.1016/j.sse.2023.108849
Received 2 November 2023; Received in revised form 11 December 2023; Accepted 12 December 2023
Available online 21 December 2023

Table 1
Model Parameters. All the parameters of DGFET and SGFET are the same of [2] and [4] respectively.

	DGFET	SGFET
L [μm]	1	1
t_{Si} [nm]	5	—
R [nm]	—	2.5
t_{OX} [nm]	1.5	1.5
μ [cm^2/Vs]	300	300
Δψ [V]	0	0
ε_{Si}	11.7	11.7
ε_{OX}	3.9	3.9

2. DGFET

In the DGFET, the channel is conventionally undoped (or lightly doped) to avoid fluctuations of the threshold voltage. Here, the device geometry and all the symbols are exactly the same of the well-known paper of Taur [2] (Fig. 1). Assuming the current flowing in the y-direction, in order to compute the surface potential, the Poisson's equation must be solved. The Poisson's equation is solved following the same approach of Taur [2]. The solution of the Poisson's equation without introducing any approximation reads

$$\frac{q(V_{GS}-\Delta\psi-V)}{2kT}-\ln\left[\frac{2}{t_{si}}\sqrt{\frac{2\varepsilon_{si}kT}{q^2n_i}}\right]=\ln\beta-\ln[\cos\beta]+\frac{2\varepsilon_{si}t_{ox}}{\varepsilon_{ox}t_{si}}\beta\tan\beta \tag{1}$$

where β is an intermediate parameter to be determined by solving the transcendental equation (1), q is the electron charge, k the Boltzmann constant, T the lattice temperature, $\Delta\psi$ is the work-function difference between the gate electrode and the intrinsic silicon, V is the channel potential, n_i is the intrinsic concentration, ε_{ox} is the insulator dielectric constant, ε_s is the silicon dielectric constant, t_{ox} is the insulator thickness, t_{si} is the semiconductor thickness, V_{GS} is the voltage applied to the gate. Once β is computed, the electrostatic potential normal to the channel (x-direction) in the semiconductor reads [2]

$$\psi(x)=V-\frac{2kT}{q}\ln\left[\frac{t_{si}}{2\beta}\sqrt{\frac{q^2n_i}{2\varepsilon_{si}kT}}\cos\left(\frac{2\beta x}{t_{si}}\right)\right] \tag{2}$$

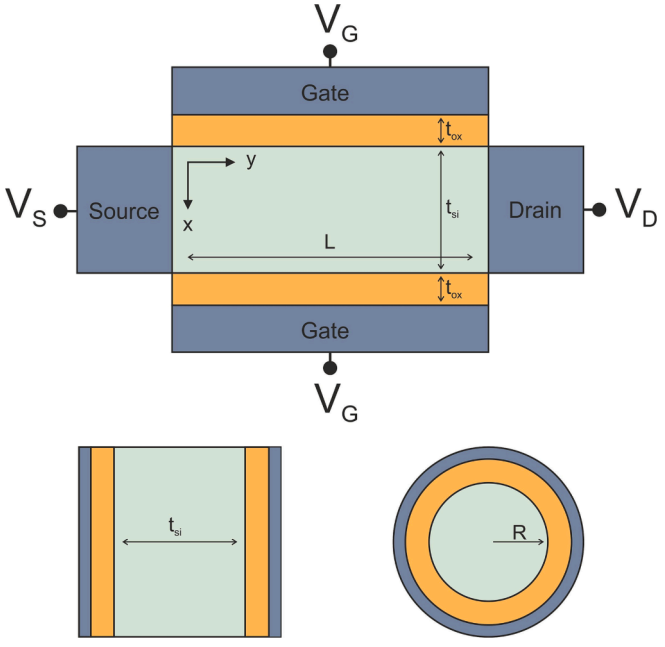

Fig. 1. Schematic structure of DGFET (left) and SGFET (right).

and, in turn, the mobile charge in the channel [2]:

$$Q_i=C_{ox}(V_{GS}-\Delta\psi-\psi_s)=2\varepsilon_{si}\frac{2kT}{q}\frac{2\beta}{t_{si}}\tan\beta \tag{3}$$

where $\psi_s=\psi(\pm t_{si}/2)$ and $C_{ox}=\varepsilon_{ox}/t_{ox}$. To work out a surface potential formulation of the drain current, we recall that the charge sheet approximation (CSM), widely used for planar MOSFET modeling, is not suitable for DGFETs [2]. Dealing with DGFETs, in fact, the exact solution Pao-Sah equation is mandatory to accurately model the volume inversion in the subthreshold region [2,5,6]. Nevertheless, the Pao-Sah double integral, can be worked out to be a function of the surface potential ψ_s, without introducing any simplification [5]-[6]

$$I_D=-W\mu Q_i\frac{dV}{dy}=-W\mu\left(\widetilde{Q}_i\frac{d\psi_s}{dy}-v_T\frac{dQ_i}{dy}\right) \tag{4}$$

where $v_T=kT/q$ is the thermal voltage, and

$$\widetilde{Q}_i=Q_i\left[1+\frac{\gamma}{4}g(\beta)\right] \tag{5}$$

can be seen as a perturbed inversion charge and

$$g(\beta)=\frac{\sin(2\beta)-2\beta\cos(2\beta)}{\beta\tan(\beta)[2\beta+\sin(2\beta)]},\quad \gamma=\frac{\varepsilon_{ox}t_{si}}{\varepsilon_{si}t_{ox}} \tag{6}$$

Thanks to eq. (4), the drain current is computed by means of the surface potential ψ_s [5,6], without invoking the charge sheet approximation, typically used in compact models. From the physical standpoint, the difference between Q_i and $\widetilde{Q}_i$ accounts for the fact that, in the DGFET, the current is not confined to a narrow surface channel. Conventionally, to work out the drain current, Q_i, $\widetilde{Q}_i$, are regionally simplified [2,3] or linearized as in the SLM and PSP [5,6]. In this work it is interpolated by means of a second order symmetric polynomial centered at the surface potential midpoint $\psi_M=(\psi_{sS}+\psi_{sD})/2$, [17]. This approach gives a more accurate and significantly simplified version of drain current and terminal charges with respect to the existing core models of DGFET, while keeping a clear physical nature. As shown in eq. (5), $\widetilde{Q}_i$ can be viewed as a slightly perturbed formulation of Q_i, [5,6]. Unfortunately, despite Q_i, $\widetilde{Q}_i$ is a nonlinear function of ψ_S. To integrate eq. (4) we observe that $\widetilde{Q}_i$ is slightly nonlinear (Fig. 2) and can be very well approximated with a second order polynomial P_Q as follows

$$\widetilde{Q}_i\cong P_Q(s)=\widetilde{Q}_{iM}+\widetilde{A}s+\widetilde{B}s^2 \tag{7}$$

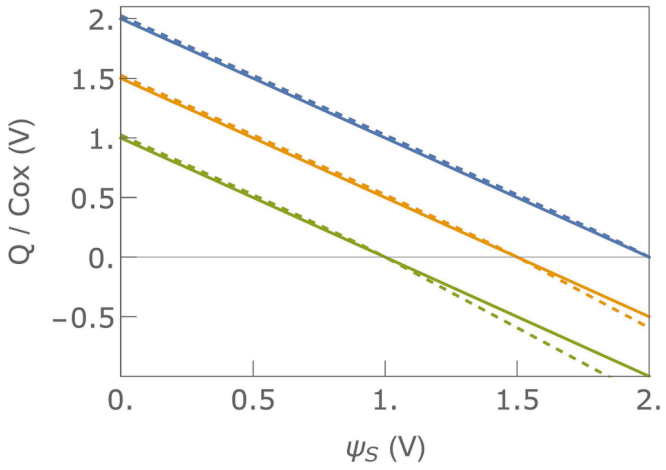

Fig. 2. Inversion charge in the channel Q_i (solid line) and $\widetilde{Q}_i$ (dashed line) vs. surface potential at V_{GS} = 3 V (blue), 2 V (orange), 1 V (green). Simulation parameters are shown in tab.1.

where $\widetilde{Q}_{iM} = \widetilde{Q}_i(\psi_M)$, $s = \psi_s - \psi_M$, ψ_{sS} and ψ_{sD} are the surface potential at the source and drain contacts, respectively. $\widetilde{A}$, $\widetilde{B}$ are calculated equating $\widetilde{Q}_{iS} = P_Q(-\phi/2)$, $\widetilde{Q}_{iD} = P_Q(\phi/2)$: $\widetilde{A} = (\widetilde{Q}_{iD} - \widetilde{Q}_{iS})/\phi$, $\widetilde{B} = 2(\widetilde{Q}_{iS} + \widetilde{Q}_{iD} - 2\widetilde{Q}_{iM})/\phi^2$, $\phi = \psi_{sD} - \psi_{sS}$ and $\widetilde{Q}_{iS}$, $\widetilde{Q}_{iD}$ are the perturbed inversion charges at source and drain respectively [5,17]. Finally, since Q_i is linear (3), it can be straightforwardly worked out as a function of s without additional simplifications

$$Q_i = C_{ox}(V_{GS} - \Delta\psi - \psi_s \pm \psi_M) = Q_{iM} - C_{ox}s \tag{8}$$

where $Q_{iM} = C_{ox}(V_{GS} - \Delta\psi - \psi_M)$. It is worth stressing that, apart the approximation $P_Q(s)$, no other simplification is used in this work to compute currents, terminal charges, and capacitances.

Substituting eqs. (7) and (8) in the R.H.S of eq. (4) and observing that $ds = d\psi_s$, $dQ_i = -C_{ox}ds$, and that the device is symmetric, the drain current turns out to be a polynomial function of s only

$$I_D\, dy = 2W\mu\left[\widetilde{Q}_{iM} + \widetilde{A}\, s + \widetilde{B}\, s^2 + C_{ox}\, v_T\right] ds \tag{9}$$

Integrating eq. (9) and replacing the corresponding value of s at the source ($s = -\phi/2$) and drain ($s = \phi/2$), the current eventually turns out to be [17]

$$I_D = 2\frac{W}{L}\mu\left[\frac{4\widetilde{Q}_{iM} + \widetilde{Q}_{iD} + \widetilde{Q}_{iS}}{6} + C_{ox}v_T\right]\phi \tag{10}$$

where $\widetilde{Q}_{iM} = Q_{iM}\left[1 + \frac{\gamma}{4}g(\beta_M)\right]$, $Q_{iM} = C_{ox}(V_{GS} - \Delta\psi - \psi_M)$ and ϕ, $\widetilde{Q}_{iS}$, $\widetilde{Q}_{iD}$, are explicit functions of β that, in turn, is an implicit function of V_S, V_D, V_{GS}. β_S, β_D, and β_M must be computed by numerical iteration with eq. (2) and (3) respectively. Nevertheless, several excellent explicit approximations of β are reported in the literature [18]. The neat mathematical formulation of eq. (10) and its high accuracy, combined with the accurate explicit approximation of β, make this model very suitable for circuit simulation programs. Besides, eq. (10) does not require computing the derivative of the charge at the surface potential midpoint [5,6].

The derivative, actually, is cumbersome, requires simplifications and careful coding when implemented into a circuit simulator to avoid singularities or imaginary solutions through the numerical iterations. To assess the overall accuracy of this compact model, in Fig. 3 eq. (10) is compared with the exact numerical solution of the Pao-Sah integral [2], and with the simplified compact model in [3 eq. (9)]. In Fig. 3 the corresponding percentage errors, defined as $100 \times |(\Delta I_{DS})/I_{DS}|$, is shown. It is worth remembering that all the device parameters and terminal voltages are exactly the same of ref. [2]. In [2], in turn, the analytic solution is compared with numerical simulations and experiments. This model gives a smooth, continuous, and very accurate expression of currents, charges, and their first order derivatives as well as of the higher order derivatives [17]. Furthermore, eq. (10) passes all the higher order Gummel symmetry tests [17]. These features are important to achieve a rapid and smooth convergence of circuit simulations and to implement SCE. Eq. (10), despite its simple linear formulation, reproduces the exact numerical solution with a maximum percentage error of about of 0.1 % (Fig. 3, 4, 5): it is more than one order of magnitude smaller with respect to the well-known compact models in [3,5]. The transfer characteristic is shown in Fig. 4. Finally, in Fig. 5 the model is compared with the numerical solution at different device parameters.

3. SGFET

An analogous formulation, following the same approach, can be worked out for the SGFET. Let us consider the undoped (lightly doped) cylindrical n-type SGFET of radius R of Fig. 1. The device geometry and

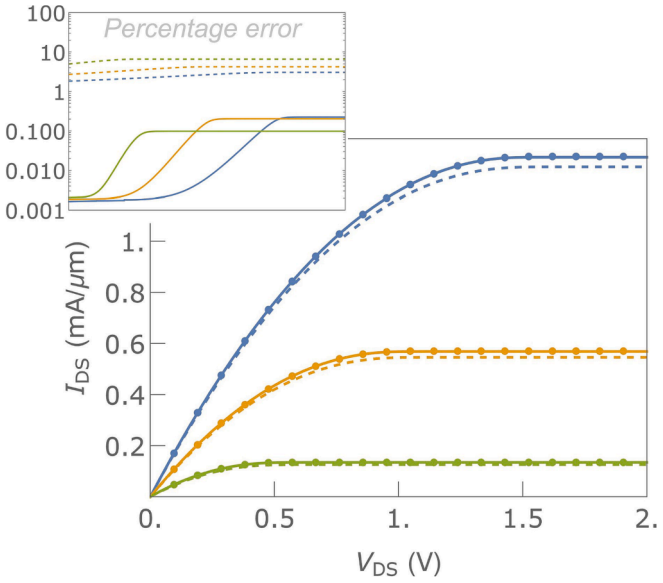

Fig. 3. Output currents of the DGFET and corresponding percentage error at V_{GS} = 2 V (blue), 1.5 V (orange), 1 V (green). Solid lines exact numerical solution, dots eq. (10), dashed line the approx. [3]. Simulation parameters are shown in tab.1.

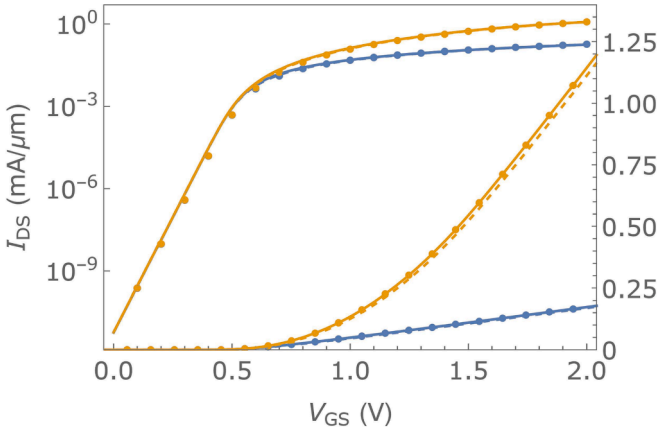

Fig. 4. Transfer characteristics at V_{GS} = 0.1 V (blue), 1 V (orange). Solid lines exact numerical solution, dots eq. (10), dashed line the approx. As shown in Fig. 3, below threshold the percentage error is smaller than 10^{-2} %. Simulation parameters are shown in tab.1.

symbols are the same of [4]. Assuming the transport in the y-direction, ($0 < r < R$ is the direction normal to the current) the solution of the Poisson's equation reads [4]:

$$\frac{q(V_{GS} - \Delta\psi - V)}{kT} - \ln\left(\frac{8}{\delta R^2}\right) = \ln(1-\beta) - \ln\beta^2 + \eta\left(\frac{1-\beta}{\beta}\right) \tag{11}$$

where $\eta = 4\varepsilon_{si}/(C_{ox}R)$, and $\delta = q^2 n_i/(kT\varepsilon_{si})$. All the other parameters have the same meaning of the DGFET. Again, knowing β after solving the transcendental eq. (11), the potential in the semiconductor as a function of r can be straightforwardly calculated [4]:

$$\psi(r) = V + \frac{kT}{q}\ln\left(\frac{-8B}{\delta(1 + Br^2)^2}\right) \tag{12}$$

And, in turn, the inversion charge

$$Q_i = C_{ox}(V_{GS} - \Delta\psi - \psi_s) = 2\varepsilon_{si}\frac{2kT}{q}\frac{1}{\beta R}(1-\beta) \tag{13}$$

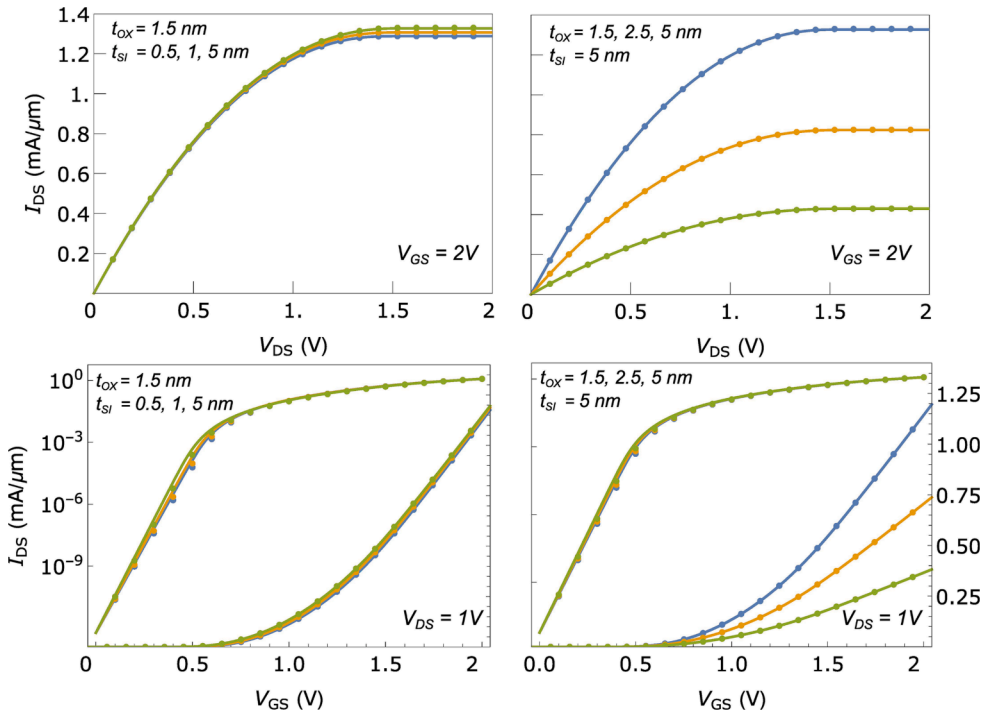

Fig. 5. Output and transfer characteristics at different layers thickness. Solid lines exact numerical solution, dots eq. (10). The largest percentage error is smaller than 0.1%.

where $C_{ox} = \varepsilon_{ox}/[R\ln(1 + t_{ox}/R))]$, $\psi_s = \psi(R)$, and $\beta = 1 + BR^2$. The expression of Pao-Sah's integral, as a function of the surface potential, for a cylindrical undoped SGFET reads [5]

$$I_D = 2\pi R\mu Q_i \frac{dV}{dy} = 2\pi R\mu\left(\widetilde{Q}_i \frac{d\psi_s}{dy} - v_T \frac{dQ_i}{dy}\right) \tag{14}$$

where

$$\widetilde{Q}_i = Q_i\, g(\beta) \tag{15}$$

$$g(\beta) = 1 + \frac{\frac{1}{\beta_S} - \frac{1}{\beta_D} + \ln\left(\frac{\beta_S}{\beta_D}\right)}{\gamma\left(\frac{1}{\beta_S^2} - \frac{1}{\beta_D^2} + \frac{2}{\beta_D} - \frac{2}{\beta_S}\right)} \tag{16}$$

and

$$\gamma = \frac{2\varepsilon_{si}}{\varepsilon_{ox}} \ln\left(1 + \frac{t_{ox}}{R}\right) \tag{17}$$

Using the same polynomial approximations of $\widetilde{Q}_i$ (eq. 7), substituting the simplified expression of the inversion charge $P_Q(s)$ in the R.H.S of eq. (14) and integrating, the drain the current eventually reads

$$I_D = \frac{2\pi R}{L}\left[\frac{4\widetilde{Q}_{iM} + \widetilde{Q}_{iD} + \widetilde{Q}_{iS}}{6} + C_{ox} v_T\right]\phi \tag{18}$$

where $\widetilde{Q}_{iM}$, $\widetilde{Q}_{iS}$, $\widetilde{Q}_{iD}$, Q_{iS}, Q_{iD} are computed by means of eqs. (11)-(13). As for the DGFET, the drain current of the SGFET (18) depends on the terminal voltages through ψ_{sS}, ψ_{sD}, ψ_M, and β. Again, eq. (18) accurately reproduces the exact numerical solution of the drain current I_D with a maximum percentage error smaller than 0.1 %. In [18], it is reported an excellent approximate solution of β for the SGFET as well. It makes this model very suitable for circuit simulation programs. In Figs. 6, 7, eq. (18) is compared with the exact numerical solution, and with the approximation [3, eq. (13)].

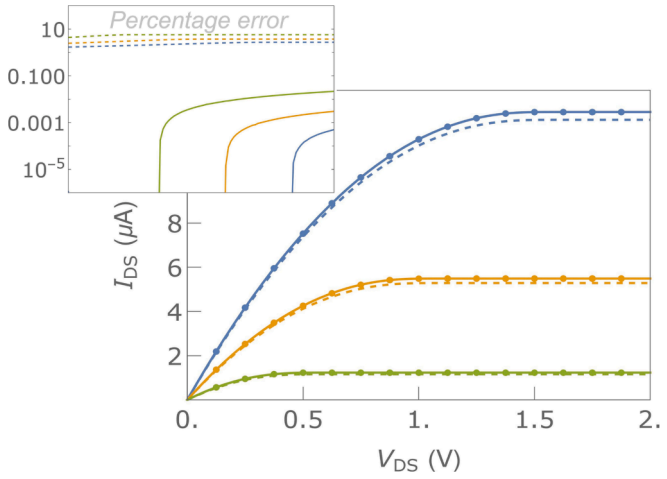

Fig. 6. Output currents of the SGFET and corresponding percentage error at V_{GS} = 2 V (blue), 1.5 V (orange), 1 V (green). Solid lines exact numerical solution, dots eq. (18) dashed line [4]. Simulation parameters are shown in tab.1.

4. Unified charge model

The most important feature of this model is the simple polynomial formulation of the charges and of the drain currents of eqs. (7), (8), (10) and (18). Despite in [2] and [4] the drain current of DGFET and SGFET is worked out exactly, they are cumbersome functions of β that cannot be used to work out the terminal charges without simplifications. In this work, instead, thanks to the polynomial expression of the inversion charge $P_Q(s)$, the quasi-static (QS) terminal charges are easily calculated without any simplification. Below, the terminal charges will be worked out for the DGFET, same expressions hold for the SGFET. The QS terminal charges are calculated using the well-known Ward–Dutton charge partitioning [16] conventionally defined as [3]

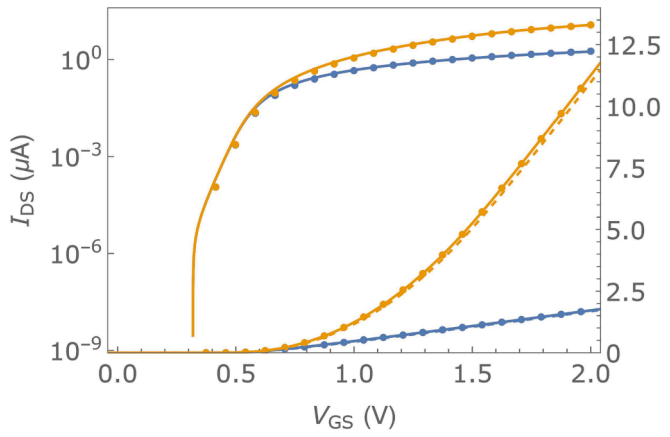

Fig. 7. Transfer characteristics at $V_{GS} = 0.1$ V (blue), 1 V (orange). Solid lines exact numerical solution, dots eq. (18), dashed line [4]. As shown in Fig. 3, below threshold the percentage error is smaller than 10^{-2} %. Simulation parameters are shown in tab.1.

$$\frac{Q_G}{2W} = \int_0^L Q_i(s)dy = \int_{-\phi/2}^{\phi/2} Q_i(s)\frac{dy}{ds}ds \tag{19}$$

$$\frac{Q_D}{2W} = \int_0^L \frac{y}{L} Q_i(s)dy = \int_{-\phi/2}^{\phi/2} \frac{y(s)}{L} Q_i(s)\frac{dy}{ds}ds \tag{20}$$

$$Q_S = Q_G - Q_D \tag{21}$$

where Q_S, Q_D, Q_G are the source, drain, and gate charge density per unit area. The above integrals are carried out analytically. First, the expression of $y(s)$ is required. Since the current in the channel is position-independent, eq. (9) can be regarded as a differential equation in the variable s. From eq. (9) one finds [17]:

$$\frac{dy}{ds} = R\left[\widetilde{Q}_{iM} + C_{ox}v_T + \widetilde{A}s + \widetilde{B}s^2\right] \tag{22}$$

where $R = 2W\mu/I_D$. Hence, integrating eq. (22)

$$y(s) = R\left[\left(\widetilde{Q}_{iM} + C_{ox}v_T\right)s + \frac{\widetilde{A}}{2}s^2 + \frac{\widetilde{B}}{3}s^3\right] + y_M \tag{23}$$

where y_M is the coordinate of the "surface potential midpoint", i.e., the y coordinate of $s = 0$, (Fig. 8). Furthermore, since $s = -\phi/2$ at $y = 0$, y_M reads

$$y_M = R\left[\frac{8\widetilde{Q}_{iM} + 12C_{ox}v_T + 5\widetilde{Q}_{iS} - \widetilde{Q}_{iD}}{24}\right]\phi \tag{24}$$

Combining eqs. (9), (10), (22)

$$Q_i(s)\frac{dy}{ds} = R(K_0 + K_1 s + K_2 s^2 + K_3 s^3) \tag{25}$$

where

$$K_0 = Q_{iM}\left(\widetilde{Q}_{iM} + v_T C_{ox}\right), \quad K_1 = \widetilde{A}Q_{iM} - v_T C_{ox}^2 - \widetilde{Q}_{iM}C_{ox} \tag{26}$$

$$K_2 = \widetilde{B}Q_{iM} - \widetilde{A}C_{ox}, \quad K_3 = -\widetilde{B}C_{ox}$$

Substituting eq. (25) into eq. (19) and integrating from $y = 0 \rightarrow s = -\psi/2$, to $y = L \rightarrow s = \psi/2$ the total inversion charge Q_G in the channel reads

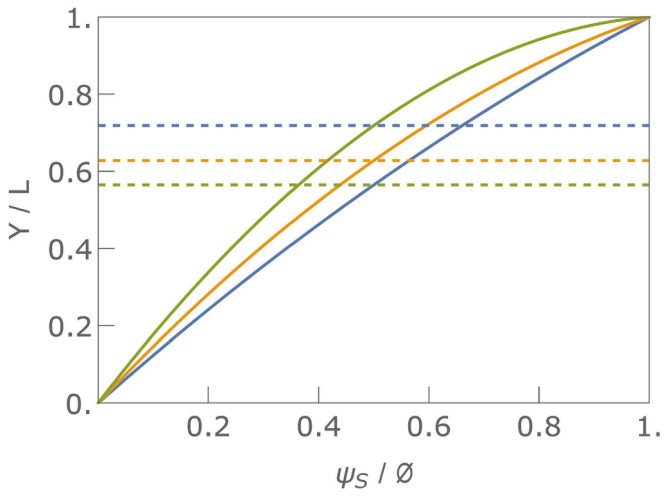

Fig. 8. Solid line, normalized position in the channel Y(s) as a function of the surface potential at $V_G = 3V$ (blue), $V_G = 2V$ (orange), $V_G = 1V$ (green), and $V_{DS} = 1V$. Dashed line, surface potential midpoint y_M. Simulation parameters are shown in tab.1.

$$Q_G = 2WR\left(K_{G1}\phi + K_{G3}\phi^3\right) \tag{27}$$

where $K_{G1} = K_0$, $K_{G3} = K_2/12$.

Substituting eqs. (23), (25), into (20) and integrating the drain charge Q_D reads

$$Q_D = 2WR\left(K_{D1}\phi + K_{D3}\phi^3 + K_{D5}\phi^5 + K_{D7}\phi^7\right) \tag{28}$$

where

$$K_{D1} = \frac{y_M K_0}{L}, \quad K_{D3} = \frac{R\widetilde{A}K_0 + 2y_M K_2 + 2RK_1\left(C_{ox}v_T + \widetilde{Q}_{iM}\right)}{24L} \tag{29}$$

$$K_{D5} = R\frac{2\widetilde{B}K_1 + 3\widetilde{A}K_2 + 6K_3\left(C_{ox}v_T + \widetilde{Q}_{iM}\right)}{480L}, \quad K_{D7} = R\frac{K_3\widetilde{B}}{1344L}$$

In Fig. 9 the terminal charges are validated by comparisons with the exact numerical solution. A very good agreement is shown. In fact, the terminal charges are worked, without introducing simplifications. Hence, the larger percentage error, with respect to the exact solution is about 0.1%, as for the drain current of eq. (10), Fig. 3: it is more than one order of magnitude smaller with respect to the well-established compact models, in [3,5]. As a double check of eqs. (28), (29), the asymptotic behavior is also shown in Fig. 9 (dashed lines). As expected, when $V_{DS} \cong 0$, the gate charge per unit width is the inversion charge density multiplied by the device length. The drain and source charges are equal and one half of the gate charge: $Q_D = Q_S = Q_G/2$. Actually, using the explicit expression of the charges in the appendix, when $V_{DS} \cong 0$, $\phi \cong 0$, $\widetilde{Q}_{iS} \cong \widetilde{Q}_{iD} \cong \widetilde{Q}_{iM}$, the terminal charges read

$$Q_G \cong 2W\frac{R}{12}G_1\phi = 2WL\frac{Q_{iM}\left(12\widetilde{Q}_{iM} + 12C_{ox}v_T\right)}{12\left(\widetilde{Q}_{iM} + C_{ox}v_T\right)} = Q_{iM} \tag{30}$$

$$Q_D \cong 2W\frac{R^2}{L}\frac{D_1}{72}\phi^2 = 2WL\frac{Q_{iM}\left(6\widetilde{Q}_{iM} + 6C_{ox}v_T\right)^2}{72\left(\widetilde{Q}_{iM} + C_{ox}v_T\right)^2} = \frac{Q_G}{2}$$

$$Q_S = Q_G - \frac{Q_G}{2} = \frac{Q_G}{2}$$

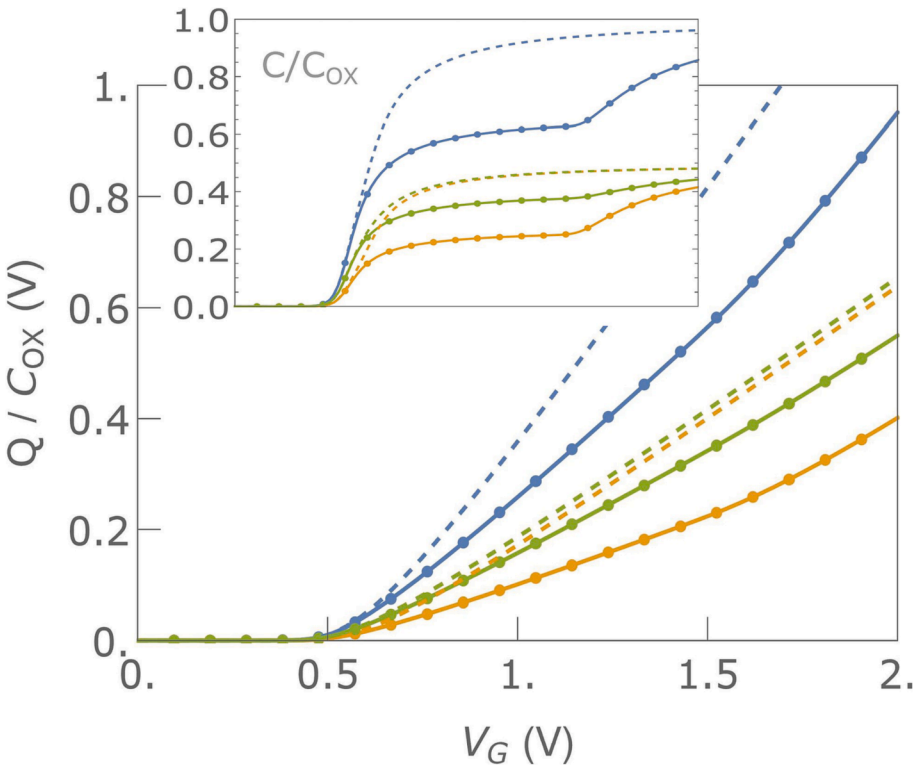

Fig. 9. Solid lines, terminal charges (27), (28) vs. numerical solution (circles) at $V_s = 0\,V$, $V_D = 1\,V$: Q_G (blue), Q_S (green), Q_D (orange). Dashed line terminal charges at $V_D = 0.1\,V$. Inset: normalized capacitance (C/C_{OX}). Solid lines C_{GG} (blue), C_{SG} (green), Q_{DG} (orange), at $V_s = 0\,V$, $V_D = 1\,V$, vs. numerical solution (circles). Dashed line capacitances (27), (28) at $V_D = 0.1\,V$. Simulation parameters are shown in tab.1.

An even more stringent test is the comparison of the transcapacitances, $C_{ij} = (2\delta_{ij} - 1)\partial Q_i/\partial V_j$, where $i, j = G, S, D$. Fig. 9 shows that the transcapacitances are essentially identical to the exact numeric solution. Again, the larger percentage error, is in the order of 0.1%.

5. Surface potential and electric field

A simple, yet exact, analytical expression of the surface potential $\phi_s(y)$, and of the electric field $E(y)$ in the channel are very useful to implement SCE and advanced physical effects. Same expressions hold for both the DGFET and the SGFET. The explicit dependence $\psi_s(y)$ is worked out by solving eq. (23) with respect to s. It is a cubic equation that has one real and two imaginary solutions. Neglecting the imaginary roots, the surface potential reads [17]

$$\psi_s = \psi_M + s = \psi_M + \frac{b + \theta + \bar{\theta}}{3a} \tag{25}$$

where

$$\theta = \left[0.5\left(\Delta_1 + \left(\Delta_1{}^2 - 4\Delta_0{}^3\right)^{1/2}\right)\right]^{1/3},$$
$$\bar{\theta} = \left[0.5\left(\Delta_1 - \left(\Delta_1{}^2 - 4\Delta_0{}^3\right)^{1/2}\right)\right]^{1/3}$$

and $\Delta_0 = b^2 - 3ac$, $\Delta_1 = 2b^3 - 9abc + 27a^2d$, $a = \widetilde{B}/3$, $b = \widetilde{A}/2$, $c = \widetilde{Q}_{iM} + C_{ox}v_T$, $d = y_M - y/R$.

Finally remembering that $E_Y = -d\psi_s/dy = -ds/dy$, thanks to eq. (22) the electric field in the channel E_Y reads [17]

$$E_Y = -\frac{ds}{dy} = -\frac{1}{R\left(\widetilde{Q}_{iM} + C_{ox}v_T + \widetilde{A}s + \widetilde{B}s^2\right)} \tag{26}$$

which, in turn, can be expressed as a function of the position in the channel replacing in (26) the expression of $s(y)$: $s = (b + \theta + \bar{\theta})/3a$.

6. Conclusions

In this work a compact core model of DGFET and SGFET suitable for advanced CAD applications is shown. It is developed based on the exact solution of the Poisson's equation without charge-sheet approximation exploiting a symmetric quadratic polynomial to interpolate the inversion charge in the channel. It gives an extremely accurate and significantly simplified version of the Pao-Sah's equation while keeping a clear physical nature. The maximum percentage error with respect the Pao-Sah's equation is in the order of 0.1% for current, terminal charges and transcapacitances: more than one order of magnitude smaller than the well-established models in [3,5]. Apart from the inversion charge interpolation, no other simplification is required to work out the terminal charges and capacitances. The model is fully scalable and is suitable full range of device geometries, from the long-channel limit down to the shortest channels, with a single set of parameters. The model, thanks to its polynomial formulation, is particularly suited to easily manage terminal charges, capacitances, small channel and quantum effects. It is a useful kernel for the future generation of SPICE models of FINFET and Nano Sheets, maintaining the same ease of implementation of today's most advanced planar MOSFET models.

CrediT authorship contribution statement

Luigi Colalongo: Conceptualization, Writing – review & editing. **Simone Comensoli:** Conceptualization, Writing – review & editing. **Anna Richelli:** Validation, Writing – review & editing.

Declaration of competing interest

The authors declare that they have no known competing financial

interests or personal relationships that could have appeared to influence the work reported in this paper.

Data availability

No data was used for the research described in the article.

Appendix

Substituting the expression of $\widetilde{A}$, $\widetilde{B}$, K_0, K_1, K_2, K_3, in eqs. (27), (28), the terminal charges Q_G, Q_D and, in turn, Q_S can be straightforwardly worked out as a function of the intrinsic charges only:

$$Q_G = 2W\frac{R}{12}\left(G_1\phi + G_2\phi^2\right) \tag{A1}$$

where

$$G_1 = Q_{iM}\left(12v_T C_{ox} + 2\widetilde{Q}_{iD} + 8\widetilde{Q}_{iM} + 2\widetilde{Q}_{iS}\right), \quad G_2 = C_{ox}\left(\widetilde{Q}_{iS} - \widetilde{Q}_{iD}\right)$$

and

$$Q_D = 2W\frac{R^2}{L}\left(\frac{D_1}{72}\phi^2 - \frac{D_2}{5040}\phi^3\right) \tag{A2}$$

where

$$D_1 = Q_{iM}\left(6v_T C_{ox} + \widetilde{Q}_{iD} + 4\widetilde{Q}_{iM} + \widetilde{Q}_{iS}\right)^2,$$

$$D_2 = C_{ox}\left[420C_{ox}^2 v_T^2 + 29Q_{iD}^2 + 144Q_{iM}^2 - 41Q_{iS}^2 + 42C_{ox}v_T\left(9\widetilde{Q}_{iD} + 12\widetilde{Q}_{iM} - \widetilde{Q}_{iS}\right) - 32\widetilde{Q}_{iM}\widetilde{Q}_{iS} + 8\widetilde{Q}_{iD}\left(31\widetilde{Q}_{iM} + 9\widetilde{Q}_{is}\right)\right]$$

References

[1] Colinge J-P. Multiple gate SOI MOSFETs. Solid State Electron June 2004;48(6): 897–905. https://doi.org/10.1016/j.sse.2003.12.020.

[2] Taur Y, Liang X, Wang W, Lu H. A continuous, analytic drain current model for DG-MOSFETs. IEEE Electron Device Lett Feb. 2004;25:107–9. https://doi.org/10.1109/LED.2003.822661.

[3] Lu H, Yu B, Taur Y. A unified charge model for symmetric double-gate and surrounding-gate MOSFETs. Solid State Electron Aug. 2008;52:67–72. https://doi.org/10.1016/j.sse.2007.06.018.

[4] Jimenez D, Iniguez B, Sune J, Marsal FL, Pallares J, Roig J. Continuous analytic current–voltage model for surrounding-gate MOSFETs. IEEE Electron Device Lett Aug. 2004;25:571–3. https://doi.org/10.1109/LED.2004.831902.

[5] Dessai G, Dey A, Gildenblat G, Smit GDJ. Symmetric linearization method for double-gate and surrounding-gate MOSFET models. Solid State Electron Feb. 2009; 53:548–56. https://doi.org/10.1016/j.sse.2009.01.020.

[6] G.D.J. Smit, A.J. Scholten, G. Curatola, R. van Langevelde, G. Gildenblat, D.B.M. Klaassen, "PSP-based scalable compact FinFET model," NSTI-Nanotech 2007, vol. 3, pp. 520–525, Feb. 2007, www.nsti.org, ISBN 1420061844.

[7] Sallese J-M, Jazaeri F, Barbut L, Chevillon N, Lallement C. A Common Core Model for Junctionless Nanowires and Symmetric Double-Gate FETs. IEEE Trans Electron Devices Dec. 2013;60(12):4277–80. https://doi.org/10.1109/TED.2013.2287528.

[8] Chevillon N, Sallese J-M, Lallement C, Prégaldiny F, Madec M, Sedlmeir J, et al. Generalization of the Concept of Equivalent Thickness and Capacitance to Multigate MOSFETs Modeling. IEEE Trans Electron Devices Jan. 2012;59(1): 60–71. https://doi.org/10.1109/TED.2011.2171347.

[9] Sallese J-M, Chevillon N, Prégaldiny F, Lallement C, Iñiguez B. The Equivalent-Thickness Concept for Doped Symmetric DG MOSFETs. IEEE Trans Electron Devices Nov. 2010;57(11):2917–24. https://doi.org/10.1109/TED.2010.2071090.

[10] Cerdeira A, Moldovan O, Iniguez B, Estrada M. Modeling of potentials and threshold voltage for symmetric doped double-gate MOSFETs. Solid State Electron May 2008;52:830–7. https://doi.org/10.1016/j.sse.2007.10.046.

[11] A. Cerdeira, B. Iníguez, M. Estrada, "Compact model for short channel symmetric doped double-gate MOSFETs," Solid-State Electron. 2008, vol. 52, pp.1064-1070, July 2008, DOI: 10.1016/j.sse.2008.03.009.

[12] Cerdeira A, Garduno I, Tinoco J, Ritzenthaler R, Franco J, Togo M, et al. Charge based DC compact modeling of bulk FinFET transistor. Solid-State Electron 2013; 87:11–6. https://doi.org/10.1016/j.sse.2013.04.028.

[13] Cerdeira A, Estrada M, Pavanello MA. On the compact modelling of Si nanowire and Si nanosheet MOSFETs. Semicond Sci Technol 2022;37:Jan. https://doi.org/10.1088/1361-6641/ac45c0.

[14] Iniguez B, Jimenez D, Roig J, Hamid HA, Marsal LF, Pallares J. Explicit continuous model for long-channel undoped surrounding gate MOSFETs. IEEE Trans Electron Devices Aug. 2005;52(8):1868–73. https://doi.org/10.1109/TED.2005.852892.

[15] Yu B, Lu W-Y, Lu H, Taur Y. Analytic charge model for surrounding-gate MOSFETs. IEEE Trans Electron Devices Mar. 2007;54(3):492–6.

[16] D. Ward, R. Dutton, "A charge-oriented model for MOS transistor capacitances," IEEE J. Solid State Circuits, vol. SSC-13, no. 5, pp. 703–708, Oct. 1978.

[17] Colalongo L, Richelli A. A Second-Order Surface Potential Core Model for Submicron MOSFETs. IEEE Trans TCAD Sept. 2022;41:2652–6. https://doi.org/10.1109/TCAD.2021.3109544.

[18] B. Yu, H. Lu, M. Liu, Y. Taur, IEEE Trans. Electron Devices, vol. 54, pp. 2715-2722, June 2007, DOI: 10.1109/TED.2007.904410.